Description of Gravity Cores from San Pablo Bay and Carquinez Strait, San Francisco Bay, California

By Donald L. Woodrow, John L. Chin, Florence L. Wong, Theresa Fregoso, and Bruce E. Jaffe

Open-File Report 2017–1078

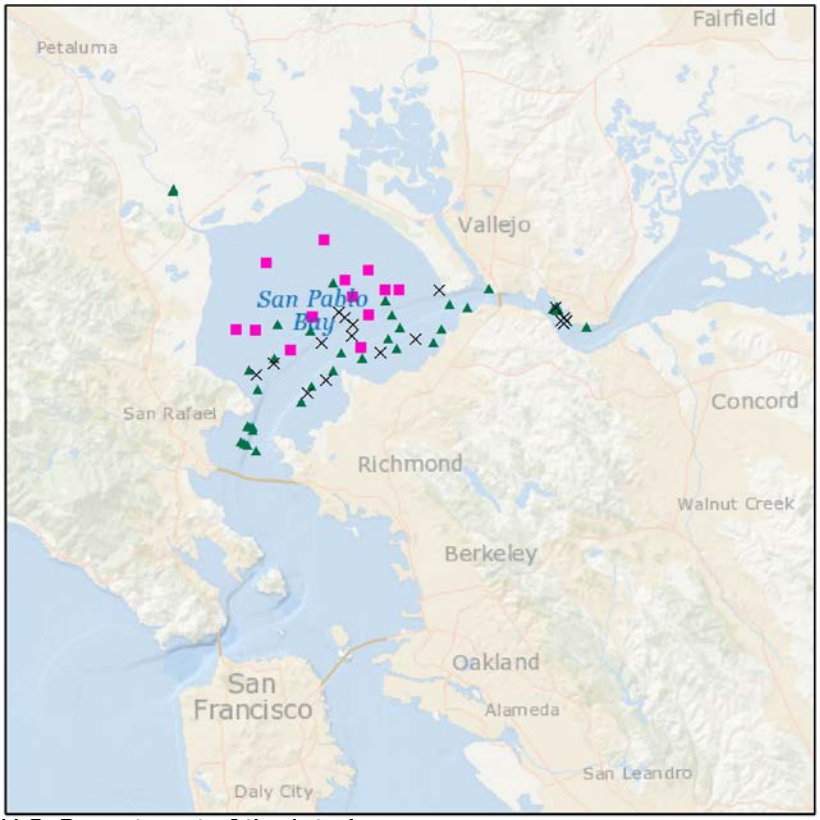

U.S. Department of the Interior
U.S. Geological Survey

Cover Image: Map of San Francisco Bay area, California, with location of gravity cores from San Pablo Bay and Carquinez Strait. See figure 1 for explanation. Basemap from Esri, Inc.

U.S. Department of the Interior

RYAN K. ZINKE, Secretary

U.S. Geological Survey

William H. Werkheiser, Acting Director

U.S. Geological Survey, Reston, Virginia: 2017

For more information on the USGS—the Federal source for science about the Earth, its natural and living resources, natural hazards, and the environment—visit https://www.usgs.gov/ or call 1–888–ASK–USGS (1–888–275–8747).

For an overview of USGS information products, including maps, imagery, and publications, visit https://www.usgs.gov/pubprod/.

Suggested citation:
Woodrow, D.L., Chin, J.L., Wong, F.L., Fregoso, Theresa, Jaffe, B.E., 2017, Description of gravity cores from San Pablo Bay and Carquinez Strait, San Francisco Bay, California: U.S. Geological Survey Open-File Report 2017–1078, 14 p., https://doi.org/10.3133/ofr20171078.

ISSN 2331-1258 (online)

Contents

Figures

Tables

Description of Gravity Cores from San Pablo Bay and Carquinez Strait, San Francisco Bay, California

By Donald L. Woodrow, John L. Chin, Florence L. Wong, Theresa Fregoso, and Bruce E. Jaffe

Abstract

Seventy-two gravity cores were collected by the U.S. Geological Survey in 1990, 1991, and 2000 from San Pablo Bay and Carquinez Strait, California. The gravity cores collected within San Pablo Bay contain bioturbated laminated silts and sandy clays, whole and broken bivalve shells (mostly mussels), fossil tube structures, and fine-grained plant or wood fragments. Gravity cores from the channel wall of Carquinez Strait east of San Pablo Bay consist of sand and clay layers, whole and broken bivalve shells (less than in San Pablo Bay), trace fossil tubes, and minute fragments of plant material.

Introduction

Seventy-two gravity cores were collected by the U.S. Geological Survey (USGS) in 1990, 1991, and 2000 from San Pablo Bay and Carquinez Strait, California (fig. 1). Fifty-six of the cores were collected in 1990 and 1991 during cruises J-2-90-SF and J-1-91-SF (Anima and others, 2005) (tables 1–3). Cores collected by Anima and others are referred to hereafter as “Anima cores.” An additional 16 gravity cores were collected in 2000 during cruise J-2-00-SF (Allison and others, 2003) and these cores are summarized in table 4. Cores collected by Allison and others are referred to hereafter as “Allison cores.” Eleven Anima cores could not be located in storage and are referred to in tables 1–3 as “no cores.” Whole-round X-radiographs are available for seven of those cores (tables 2 and 3). Logs prepared from the X-radiographs alone are referred to as “skeletal logs.” All of the Allison cores are available, eight of them with X-radiographs (table 4).

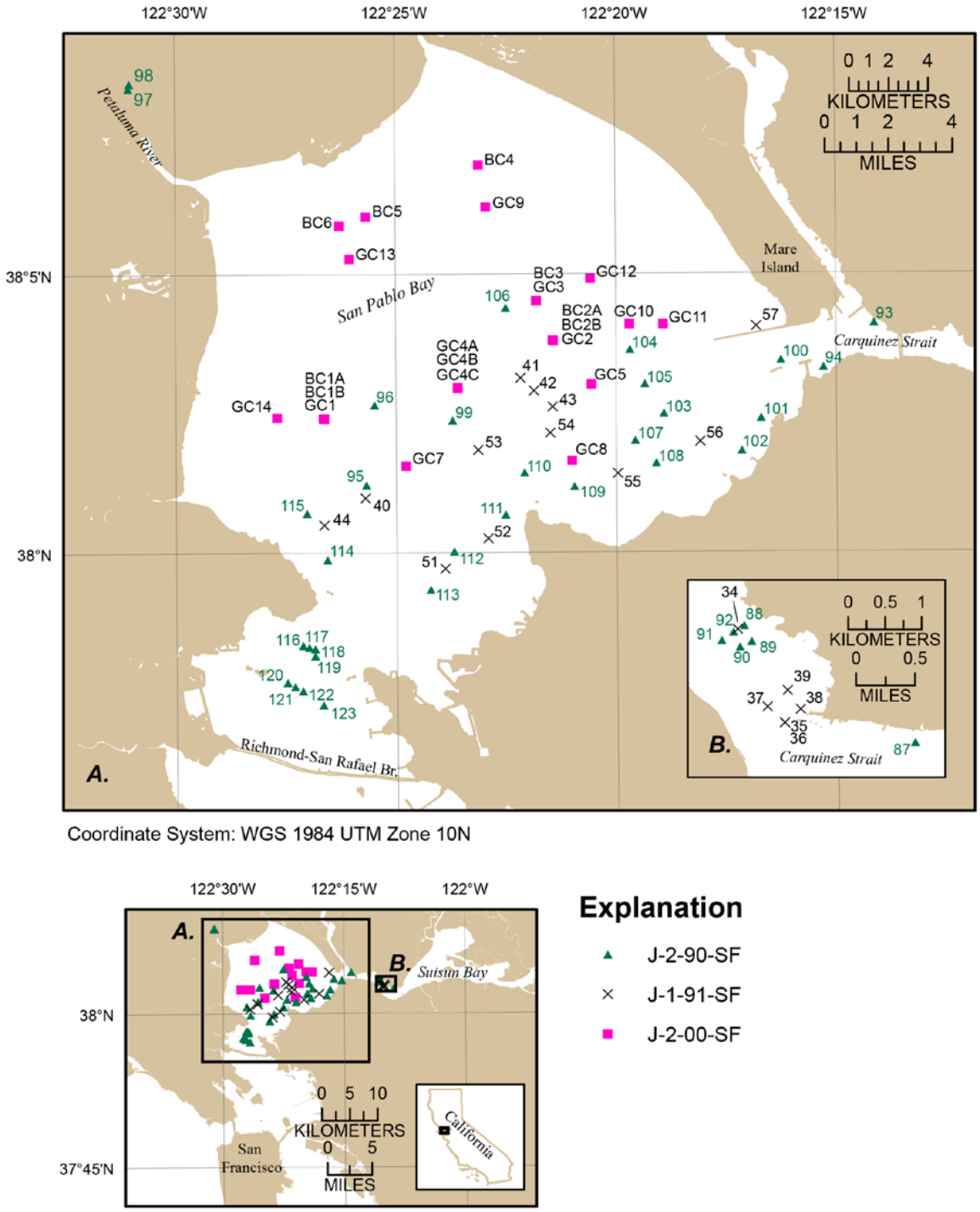

Coordinate System: WGS 1984 UTM Zone 10N

Figure 1. Maps showing locations of gravity cores collected in 1990, 1991, and 2000 by Allison and others (2003) and Anima and others (2005).

Methods and Description

Details about core collection methods are given in Anima and others (2005) and Allison and others (2003). Cores longer than 1.5 meters (m) were cut into segments of 1.5 m or less to meet the dimensions of the core-cutter in use at the USGS core analysis laboratory. The top segment of a core is referred to in the descriptions as "A" and the bottom segment as "B." The cores are stored in plastic core liners in a cold room (39°F) at the USGS storage facility at 1010–1050 O'Brien Drive, Palo Alto, Calif. Scanned copies of the core descriptions are available in the associated data release (Woodrow and Wong, 2017).

Sediments in Anima cores are slightly desiccated but the Allison cores show little desiccation. Sediments in the Anima cores are either completely oxidized or nearly so. Oxidation changes the original black or dark-gray sediment color (Munsell colors N1–N3) to dark grayish-brown or olive (Munsell colors 2.5Y–5Y). Anima cores 90-105, 90-109, and 91-44 include isolated patches of what may be the original dark-gray to black color. Allison cores show little color change. In Anima cores 90-112, 90-115, and 91-41, oxidation led to deposition on fracture surfaces of thin, bright-red films of what are believed to be crystals of microcrystalline iron oxide. In spite of alteration during storage, the cores are of great value as physical records of lithology, sedimentary structures, sedimentary sequence, and paleontology. These sedimentary features, taken together, provide a record of the environments in which the sediments were deposited.

To provide sediment surfaces for description, cores were split lengthwise into two equal segments. A working split served as the basis for core description. Loose material and gouges were scraped away from the working split with a spatula to provide a clear surface. Working under incandescent lights, sediment color was determined by removing small samples for comparison with a rock-color chart.

An archive split was left undisturbed then wrapped with plastic wrap, taped, sealed in a D-tube and returned to cold storage. After description and sampling, the working split was treated in the same manner.

The lithologic log produced for each split includes: sediment color, carbonate (HCl reaction), sulfide (HCl reaction), sedimentary structures, bedding inclination, stratal type and thickness, shell characteristics and disposition, and details of sedimentary sequence. Descriptive data were supplemented with data from X-radiographs whenever possible.

Although digital color photographs were made of all split cores, the drab, nearly uniform colors of the sediment make it difficult to see lithologic features at the scales necessary for this report so photographs are not included with the graphic logs.

Supplementing lithologic descriptions with data from X-radiographs provides the best basis for assessing these fine-grained sediments. Details of bed geometry and bed relations, positions of shells, the type, position and scale of burrows, deformed strata, and erosion surfaces can be seen best in X-radiographs.

X-radiographs were obtained by using a portable veterinarian's instrument. In the absence of cores, X-radiographs served as the basis for descriptions. Descriptive logs prepared solely from X-radiographs are referred to as skeletal logs. Skeletal logs indicate stratal thickness, sedimentary structures, whole or broken shells, and the location and arrangement of shell material; but sediment color and type cannot be known with certainty.

Optical parallax reduced the value of some X-radiographs. In those cases, the length of a core illustrated in the X-radiograph does not match the length of that core as measured in the core tube. Since most cores showed little desiccation, this difference is not the result of shrinkage.

Sediment grain size was determined through use of a grain-size comparator. Most observations were made by naked eye but in a few instances a 10X hand lens was used with the grain-size comparator. However, distinguishing sediment as silty clay or clayey silt remains subjective in the absence of quantitative grain-size data. The distinction is based both on the visual aspect of the sediment and its grittiness as expressed by rubbing a small amount of sediment between thumb and index finger.

Five histograms (fig. 2) illustrate the size distribution of what appears to be sand in these sediments. Descriptive statistics for these five samples are available in table 5. The statistics demonstrate that these samples contain little sand but are actually sandy silts.

Many cores contain shell material most of which is fragmented and often size-sorted. Whole and broken articulated shells were noted in the lithologic logs. Shells and shell debris were identified to phylum level. Those few shells judged not to have been moved after death of the organism were collected for C14 analysis for age determination.

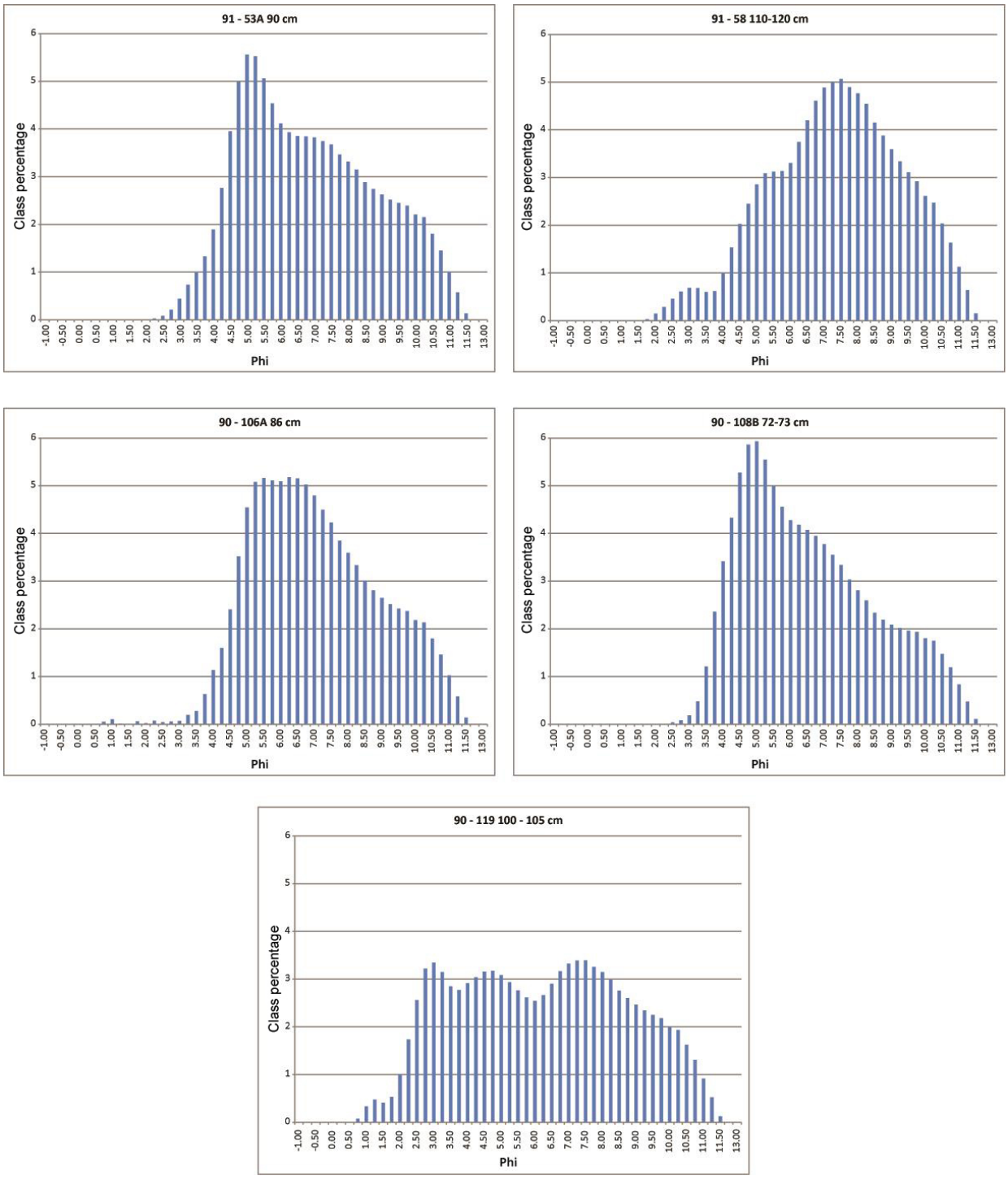

Figure 2. Histograms of the size distribution of five sandy sediment samples from Anima cores (table 5; Anima and others, 2005).

Main Features of the Sediments

San Pablo Bay

Sediments present over most of San Pablo Bay are horizontal, dark laminae of silty clay and clayey silt. By way of contrast, sediments in the San Pablo Bay channel walls, though inclined, are silty muds with little sand. Seismic-reflection studies demonstrate the existence of meter-scale, wave-like bedforms in the main channel near the Richmond-San Rafael Bridge and further east to the Carquinez Strait entrance. We lack samples to assess the sediment in the San Pablo Bay shipping channel or in the Carquinez Strait.

Silty and sandy mud, most of it bioturbated or with vague stratification, makes up as much as 90 percent of the sediment in individual cores. Erosion surfaces at many scales are seen in all of the cores. Most are minor features forming the bottom contact of thin, cross-stratified, silt laminae. More obvious erosion surfaces are evidenced by centimeter-scale, cut-and-fill structures and small channels filled with horizontal or down-lapping, silty laminae. Erosion surfaces covered by sand or sand and shell debris, some in centimeter-scale strata, rest on silty clay. These features reflect the effects of waves and tides on bottom sediments in the shallow waters of the bay as discussed by Bever and MacWilliams (2013).

The shallowest parts of the bay (water depths of 2 meters or less) fall within the tide range, which leaves large areas of bay floor subject to wave effects twice in a 24-hour period. Waves have their greatest effect on the north and northeast shores of the bay where they have shaped the arcuate shoreline. Surficial sediments of the bay are very soft and only slightly lithified, so they are easily eroded, suspended and moved by waves. Nichols and Pamatmat (1988) illustrate wintertime turbidity values much higher than those seen during the rest of the year. The greatest turbidity values are in the northern and southern parts of the bay where mudflats have developed.

Krone (1979) estimated that 15 percent of the suspended sediment seen in the bay is derived from local streams with the remainder coming from the Sacramento and San Joaquin Delta through the Carquinez Strait. Erikson and others (2013) provide a quantitative assessment for suspended sediment transport through Carquinez Strait and San Pablo Bay. Large quantities of sandy sediment were introduced to the bay in the 19th century as a result of hydraulic mining. Jaffe, Smith and Torresan (1998) illustrate changes in the bathymetry of San Pablo Bay through an analysis of depth-sounding records made over a 130-year period. Their maps illustrate deposition of sediment early in the period followed by reworking and erosion of that sediment after hydraulic mining ceased and the western Sierra streams were dammed.

Benthic life forms are responsible for many of the characteristics of the sediments in San Pablo Bay, but less so for sediments in Carquinez Strait. Whole and broken bivalve shells, burrows, and bioturbated sediment are found in most of the cores taken in shallow parts both in San Pablo Bay and Carquinez Strait. Thick-walled bivalve shells are most common in the sediments of the Strait whereas thin-walled mussel shells dominate in the muddy sediment of San Pablo Bay.

Individual trace fossils, though common, are subtle features. They are featureless tubes sectioned by the coring process and best seen in X-radiographs. Two types of tubes have been recognized in the cores. Both are circular in cross-section and a few millimeters (mm) in diameter. Tubes of one type are characterized by short, erratic paths that are closely spaced and often cut through one another (cores 90-96, 90-102, and 91-40). Another type of tube is straight, as much as 10 centimeters (cm) long (core 90-112) with a circular cross-section, and clearly defined walls. The polychaete *Sebago elongatus*, well known at many locations in San Francisco Bay,

may have formed the straight tubes. Both tube types appear to be feeding burrows as described by Seilacher (2007). The tube paths extend through strata and at the intersection of many burrows the sediment is completely homogenized.

Very small fragments of plant debris and wood are scattered through the sediment. All are dark brown or black. In a few instances organic materials make up entire laminae, but most occur as scattered millimeter-scale spots or tiny wood fragments; none are identifiable.

In addition to reworking and redistribution of sediment by wind-driven waves and tides, localized tsunamis generated by earthquakes along the Hayward, Rodgers Creek, or other local faults may have affected sediments of the bay floor. Parsons and others (2003) used hydrodynamic modeling to test the likelihood of a meter-high tsunami widely reported in San Pablo Bay after the Mare Island Earthquake of 1898. Although the model supported the possibility of such waves, the predicted amplitudes were less than those reported. Parsons and others (2003) also indicated that parts of San Pablo Bay are actively subsiding. They demonstrate that movement of fault blocks at the termination of the Rodgers Creek Fault under San Pablo Bay during the 1898 earthquake resulted in subsidence of part of the bay floor by as much as 1.5 m. Subsidence of that magnitude would provide accommodation space for sediment later deposited there thus giving support to the hypothesis of Wright and others (1992) of a pull-apart basin in the northeast part of the bay.

Laminated silts and sandy clays make up most of the sediment in the San Pablo Bay cores. Horizontally laminated sequences, small-scale cross-strata (cores 90-105, 90-108, and 91-52), and cut-and-fill structures (cores 90-99, 90-95, and 90-111) indicate the activity of bottom currents strong enough to erode and transport these fine-grained sediments. Burrows (cores 90-95, 90-115, and 91-54) are found in most strata.

Erosion surfaces are seen in most of the cores. They range from the erosional bottom contacts of individual laminae to undulose surfaces that extend into the sediment below for a centimeter or more (cores 90-99, 90-119, and 90-107). The grain size of sand resting on erosion surfaces suggests flow velocities as great as 10–20 centimeters per second (cm/sec). Higher velocities are called for in the channel where Anima and others (2005) report dunes as bedforms made up of coarse sand with mud clasts.

Although most of the sediments seen in the cores are laminated, some sections appear to be massive both in split cores or X-radiographs. These massive sections may have been bioturbated, suffered soft-sediment deformation, or both. Close inspection of some massive sections discloses tight folding, broken beds, or sharp-edged clasts of silty clay floating in a silty clay matrix (cores 90-113, 91-43, 90-93, and 90-94), all of which suggest soft-sediment deformation.

Epifauna in San Pablo Bay, according to Nichols and Pamatmat (1988), are restricted to two bivalve species and four mussel species. Nichols and Pamatmat (1988), also report the infauna of San Pablo Bay as including three amphipod species, and many species of polychaetes and oligochaetes. With this bottom-dwelling fauna, it is not surprising that many of the cored sediments exhibit evidence of bioturbation.

Shells and shell debris are important components of many cores. Most of the shells found in cores north of the channel are disarticulated, size-sorted fragments. Shells found in cores south of the channel are less often fragmented and a few shells are whole. Whole shells or shell debris are found in 10 of the 13 Anima cores taken south of the channel. Cores 91-56, 90-102, and 90-108 contain coquinas as much as 20 cm thick. Most of the 18 Allison cores have some shell debris but whole shells are found only in GC-2, GC–4B, GC 4C, and GC-7. Cores 91-56, 90-105, and 90-113 display whole shells in vertical (life?) positions.

Prior to the influx of Europeans to the San Francisco Bay Area, shellfish probably were more diverse and abundant. Native peoples around San Francisco Bay utilized shellfish as a food source as evidenced by the 400+

shellmounds they built (Nelson, 1909). Bivalves and mussels supported a 19th century shellfish industry. Present-day mining of shells near the San Mateo Bridge is an indicator of the profusion of shelly invertebrates in the older San Francisco Bay ecosystem (Hart, 1966).

Finely broken-up plant debris or wood fragments are a rare component of the sediments from north of the channel but are more common south of it. Examples are seen in Allison cores GC-2, GC-3 and Anima cores 90-40, 90-43, 90-44, 90-57, and 90-58. Minute specks of dark organic material of unknown origin are scattered throughout the sediments both north and south of the channel. In a few instances small particles of organic matter are concentrated in individual laminae. Allison core GC-19 contains a wood fragment 2 cm long.

Carquinez Strait

Carquinez Strait is a narrow (1.0–1.5 kilometers [km] wide), sinuous channel extending about 14 km from Suisun Bay on the east to San Pablo Bay on the west (fig. 1). The Strait is subject to strong ebb tides and seasonal floods from both the Sacramento and San Joaquin Rivers. Twelve Anima cores were collected on the north channel wall and on a small narrow shelf west of Benicia Point (Anima and others, 2005; fig. 1). Attempts to retrieve cores in the middle of the channel were unsuccessful. Grab samples in the main channel disclosed sand and fine gravel.

Six of the Anima cores (90-91, 90-92, 91-36, 91-37, 91-38, and 91-39) were collected either on the north side of the channel wall or at the base of the channel. All are made up of inclined strata containing couplets of fine/medium-grained sand overlain by mud. The inclined strata were most likely deposited as accretion sets developed on channel walls, or as cross-strata in large bedforms like those described by Collinson and others (2006), Kostic and Aigner (2007), and Dykstra and Kneller (2009), or both.

A second group of Anima cores (90-87, 90-88, 90-91, 91-34, 91-35) collected near the top of the channel wall or in the nearby shallows, contain couplets of silty clay above fine sand laminae arrayed as horizontal strata. Sand dominates in the couplets.

Small-scale cross-strata are prominent but rare features of the Carquinez Strait cores. They occur in fine sands and silts in sets less than 2 cm thick in cores 90-87, 90-88, 90-90, and 91-36.

Folded strata are seen in cores 91-36 and 90-88. Some strata are broken or otherwise disrupted as shown in core 91-34. The folded and broken strata appear to be the result of soft-sediment deformation.

Most sand beds in both groups of cores rest on sharp basal surfaces, some with small channel forms. Upper surfaces of these sand beds grade into mud but the mud above a few of the sand beds is thin, does not grade into the sands but appears to be draped over the underlying sand bed.

Sediment colors are dark-gray to olive-brown and probably reflect oxidation of what were once darker-colored sediments. Apparent remnants of the original, unoxidized sediments may be seen in the isolated, dark-colored masses in cores 91-36 and 91-39.

Whole bivalve shells (core 90-87) and bivalve shell debris are less common than those seen the San Pablo Bay cores. Examples of shell material in the Carquinez Strait cores are found in the upper parts of cores 90-88 and 90-90. Trace fossils seen in Carquinez Strait cores are common but are small, just a few centimeters in length. Plant material occurs as minute fragments in most cores.

Conclusion

Descriptions of 72 gravity cores demonstrate that flat-lying strata of bioturbated, silty gray mud are the norm over most of San Pablo Bay and Carquinez Strait. Sand beds are rare in the bay and strait but sand with some gravel is found on the floor of the shipping channel. Unlike the flat-lying strata found over most of the bay and strait, some of the strata in the channel walls are inclined.

Acknowledgments

We thank Michael Torresan for his help with all matters concerning accessing, manipulating and storing of cores and Angela Tan for grain-size analyses, promptly done. Special thanks go to Roberto Anima and Edward Clifton who collected the cores and provided excellent field notes. Kevin Orzech provided logs of some of the cores. Though we could not take full advantage of the technology, we thank Brian Edwards for the coaching and guidance on the graphic logging system. Mary McGann and Peter Dartnell provided timely and very helpful reviews. Woodrow appreciates the many contributions and patience of his co-authors.

References Cited

Allison D., Hampton, M., and Jaffe, B., 2003, Preliminary analysis of cores from north San Francisco Bay, California—Project description and example of data sets: U.S. Geological Survery Open-File Report 03-111, 9 p. [Also available at https://pubs.usgs.gov/of/2003/0111/]

Anima, R.J., Clifton, H.E., Reiss, Carol, and Wong, F.L., 2005, Locations and descriptions of gravity, box, and push cores collected in San Francisco Bay between January and February, 1990 and 1991: U.S. Geological Survey Open-File Report 2005-1453, 63 p. [Also available at https://pubs.er.usgs.gov/publication/ofr20051453]

Bever, A.J., and MacWilliams, M.I. 2013, Simulating sediment transport processes in San Pablo Bay using coupled hydrodynamic, waves, and sediment transport models, *in*: Barnard, P.L., Jaffe, B.E., and Schoellhamer, D.H., eds., A multi-discipline approach for understanding sediment transport and geomorphic evolution in an estuarine-coastal system—San Francisco Bay: Marine Geology, v. 345, p. 235–253. [Also available at https://doi.org/10.1016/j.margeo.2013.06.012]

Collinson, J., Mountney, N., and Thompson, D., 2006, Sedimentary structures, 3rd edition: Edinburgh, Scotland, Dunedin Academic Press, 290 p.

Dykstra, Mason, and Kneller, Ben, 2009, Lateral accretion in a deep-marine channel complex— Implications for channellized flow processes in turbidity currents: Sedimentology, v. 56, no. 5, p. 1411–1432. [Also available at https://doi.org/10.1111/j.1365-3091.2008.01040.x]

Erikson, L.H., Wright, S.A., Elias, E., Hanes, D.M., Schoellhamer, D.H, and Largier, J., 2013, The use of modeling and suspended sediment concentration measurements for quantifying net suspended sediment transport through a large tidally dominated inlet: Marine Geology, v. 345, p. 96–112. [Also available at https://doi.org/10.1016/j.margeo.2013.06.001]

Hart, E.W., 1966, Shell Deposits of southern San Francisco Bay: California Division of Mines and Geology, Mineral Information Service, v. 19, no. 3, p. 41–45.

Jaffe, B.E., Smith, R.E., and Torresan, L.Z., 1998, Sedimentation and bathymetric change in San Pablo Bay, 1856-1983: U.S. Geological Survey Open-File Report 98–759, poster 34x26 inches. [Also available at https://pubs.usgs.gov/of/1998/0759/]

Kostic, Boris, and Aigner, Thomas, 2007, Sedimentary architecture and 3D ground-penetrating radar analysis of gravelly meandering river deposits (Neckar Valley, SW Germany): Sedimentology, v. 54, no. 4, p. 789–808. [Also available at https://doi.org/10.1111/j.1365-3091.2007.00860.x]

Krone, R.B., 1979, Sedimentation in the San Francisco Bay system, *in* Conomos,T.J., Leviton, A.E., and Berson, M., eds., San Francisco Bay, the urbanized estuary; investigations into the natural history of San Francisco Bay and Delta with reference to the influence of man, (papers presented at symposium 12-16 June, 1977, San Francisco, Calif.), American Association for the Advancement of Science, Pacific Division, p. 85–96.

Nelson, N.C., 1909, Shellmounds of the San Francisco Bay region: University of California Publications in American Archeology and Ethnology, v. 7, no. 4, p. 309–356.

Nichols, F.H., and Pamatmat, M.M., 1988, The ecology of the soft-bottom benthos of San Francisco Bay—A community profile: U.S. Fish and Wildlife Service Biological Report 85(7.19), 73 p. [Also available at https://pubs.er.usgs.gov/publication/70074645]

Parsons, Tom, Sliter, Ray, Geist, E.L., Jachens, R.C., Jaffe, B.E., Foxgrover. Amy, Hart, P.E., and McCarthy, Jill, 2003, Structure and mechanics of the Hayward-Rodgers Creek Fault step-over, San Francisco Bay, California: Bulletin of the Seismological Society of America, v. 93, no. 5, p. 2187–2200. [Also available at https://doi.org/10.1785/0120020228]

Seilacher, Adolf, 2007, Trace fossil analysis: Berlin, Springer, 226 p.

Woodrow, D.L., Chin, J.L., Wong, F.L., Fregoso, T.A., Jaffe, B.E., 2017, Gravity cores from San Pablo Bay and Carquinez Strait, San Francisco Bay, California: U.S. Geological Survey data release, accessed June 23, 2017 at http://dx.doi.org/10.5066/F7XG9PB0.

Wright T.L., Smith, Neal, and Borchardt, Glenn, 1992, Right step from the Hayward Fault to the Rodgers Creek Fault beneath San Pablo Bay, *in,* Borchardt, G., Hirschfeld, S.E., McClellan, P., Williams, P. L., and Wong, J.G., eds., Proceedings of the second conference on earthquake hazards in the eastern San Francisco Bay area: California Division of Mines and Geology Special Publication, v. 113, p. 407–417.

Table 1. Carquinez Strait Anima sediment cores collected in 1990 and 1991 (Anima and others, 2005) and corresponding X-radiographs of cores. [A, top segment of core; B bottom segment of core. Y, yes; N, no.]

Core and X-radiograph number	Core Segments	Physical core available to log Y/N	X-radiograph data in the log Y/N
90-87	one	Y	Y
90-88	A and B	A and B	A - Y , B – N
90-89	one	Y	N
90-90	A and B	A – N, B – Y	A – Y, B – N
90-91	one	Y	Y
90-92	one	Y	Y
91-34	one	Y	N
91-35	one	Y	Y
91-36	A and B	A-Y, B-N	Y
91-37	one	Y	Y
91-38	A and B	Y	Y
91-39	A and B	Y	Y

Table 2. San Pablo Bay Anima sediment cores collected in 1990 (Anima and others, 2005) and corresponding X-radiographs of cores. [A, top segment of core; B bottom segment of core. Y, yes; N, no.]

Core and X-radiograph number	Core Segments	Physical core available to log Y/N	X-radiograph data in the log Y/N
90-93	None available	No core	Y
90-94	A and B	Y	Y
90-95	A and B	Y	Y
90-96	A and B	No cores	Y
90-97	None available	No core	
90-98	None available	No core	
90-99	A and B	Y	Y
90-100	None available	No core	
90-101	one	No core	Y
90-102	A and B	Y	Y
90-103	None available	No core	Y
90-104	A and B	A – Y, B – N	Y
90-105	A and B	Y	Y
90-106	A and B	A – N, B – Y	Y
90-107	A and B	A – Y, B – N	Y
90-108	A and B	Y	Y
90-109	A and B	Y	N
90-110	one	No core	Y
90-111	A and B	Y	Y
90-112	A and B	Y	Y
90-113	A and B	A – N, B – Y	A – Y, B – N
90-115	A and B	Y	Y
90-114	one	Y	N
90-116	None available	No core	N
90-117	None available	No core	N
90-118	one	No core	Y
90-119	one	Y	Y
90-120	A and B	Y	Y
90-121	A and B	Y	Y
90-122	one	Y	Y
90-123	A and B	Y	Y

Table 3. San Pablo Bay Anima sediment cores collected in 1991 (Anima and others, 2005) and corresponding X-radiographs of cores. [A, top segment of core; B bottom segment of core. Y, yes; N, no.]

Core and X-radiograph number	Core Segments	Physical core available to log Y/N	X-radiograph data in the log Y/N
91-40	one	Y	Y
91-41	A and B	Y	Y
91-42	None available	Y	Y
91-43	A and B	Y	Y
91-44	A and B	No cores	N
91-51	one	Y	Y
91-52	one	Y	N
91-53	A - Y, B - N	A – Y, B - N	Y
91-54	one	Y	Y
91-55	one	Y	Y
91-56	one	Y	N
91-57	A and B	Y	Y

Table 4. San Pablo Bay Allison sediment cores collected in 2000 (Allison and others, 2004) and corresponding X-radiographs of cores. Four cores were taken at site GC-4. Cores GC-4A and GC-4B each consist of two segments. Core GC-4C consists of three segments. [A, top segment of core; B bottom segment of core; C bottom-most segment if present. Y, yes; N, no.]

Core and X-radiograph Number	Core Segments	Physical core available to log Y/N	X-radiograph data in the log Y/N
GC-1	one	Y	Y
GC-2	A, B	Y	Y
GC-3	A, B	Y	Y
GC-4A	A, B	Y	Y
GC-4B	A, B	Y	Y
GC-4C	A, B, C	N	N
GC-5	A, B	N	N
GC-7	A, B	Y	Y
GC-8	A, B	N	N
GC-9	A, B	N	N
GC-10	A, B	Y	N
GC-11	A, B	Y	N
GC-12	A, B	Y	N
GC-13	A, B	Y	N
GC-14	A, B	Y	N
GC-15	A, B	Y	N

Table 5. Grain size data for selected samples from Anima cores collected in 1990 and 1991 (Anima and others, 2005).

Core ID, depth of sample	Folk and Ward (phi)					Inman (phi)						Trask (mm)				
	Median	Mean	Sorting	Skew	Kurtosis	Median	Mean	Sorting	Skew1	Skew2	Kurtosis	Median	Mean	Sorting	Skewness	Kurtosis
91-53A 90 cm	6.50	6.75	2.06	0.18	0.82	6.50	6.88	2.19	0.17	0.27	0.44	0.01	0.02	2.98	0.79	0.27
91-58 110-120 cm	7.30	7.26	2.00	-0.04	0.93	7.30	7.24	2.07	-0.03	-0.07	0.53	0.01	0.01	2.62	1.04	0.19
90-106A 86 cm	6.72	6.95	1.90	0.18	0.88	6.72	7.06	2.00	0.17	0.29	0.48	0.01	0.01	2.61	0.80	0.26
90-108B 72-73 cm	6.09	6.41	2.02	0.25	0.87	6.09	6.58	2.13	0.23	0.41	0.48	0.01	0.02	2.80	0.73	0.28
90-119B 100-105 cm	6.12	6.08	2.63	0.00	0.78	6.12	6.05	2.87	-0.02	0.04	0.37	0.01	0.03	4.17	1.14	0.20

ISSN 2331-1258 (online)
https://doi.org/10.3133/ofr20171078